Applied Catalysis B: Environmental 163 (2015) 554–563

Contents lists available at ScienceDirect

Applied Catalysis B: Environmental

journal homepage: www.elsevier.com/locate/apcatb

Rapid screening of silver nanoparticles for the catalytic degradation of chlorinated pollutants in water

Ottavio Lugaresi[a], Juan V. Perales-Rondón[b], Alessandro Minguzzi[a], Jose Solla-Gullón[b], Sandra Rondinini[a], Juan M. Feliu[b], Carlos M. Sánchez-Sánchez[c,d,*]

[a] Dipartimento di Chimica, Università degli Studi di Milano, Via Golgi 19, 20133 Milano, Italy
[b] Instituto Universitario de Electroquímica, Universidad de Alicante, Ap. 99, 03080 Alicante, Spain
[c] Sorbonne Universités, UPMC Univ Paris 06, UMR 8235, Laboratoire Interfaces et Systèmes Electrochimiques, F-75005 Paris, France
[d] CNRS, UMR 8235, LISE, F-75005 Paris, France

ARTICLE INFO

Article history:
Received 30 June 2014
Received in revised form 6 August 2014
Accepted 19 August 2014
Available online 27 August 2014

Keywords:
Dehalogenation
SECM
Trichloromethane
Screen-printed electrodes
Silver

ABSTRACT

Electrochemical abatement of volatile polychlorinated organic compounds for environmental applications represents a very attractive and feasible alternative for working at mild reaction conditions and reduced costs. We present herein the synthesis of three different sized Ag nanoparticles (NPs) and their electrocatalytic performance in the degradation of a model pollutant (trichloromethane, $CHCl_3$) in aqueous media. Two different methodologies are used: A conventional study based on voltammetry and chronoamperometry and a novel screening approach based on the micropipette delivery/substrate collection (MD/SC) mode of the scanning electrochemical microscopy (SECM). This new approach allows to dose any reactant, in this case $CHCl_3$, even if the latter cannot be electrogenerated. Moreover, we introduce here a novel platform for studying nanomaterials by reducing the current collector background contribution using disposable screen-printed array electrodes. The performance ranking obtained by the SECM for the three different samples of Ag NPs synthesized is validated by its comparison with the results obtained by chronoamperometry, which demonstrates the feasibility and the good sensitivity of SECM in electrocatalysts screening for the $CHCl_3$ reduction reaction. In addition, SECM allows to analyze simultaneously a large number of catalysts in one single experiment under constant experimental conditions. We suggest the proper size range and the presence of abundant superficial defective sites, such as steps or kinks, as the main reasons for Ag NPs C1 exhibiting the best overall catalytic performance in trichloromethane electrochemical reduction.

1. Introduction

Environmental electrochemistry covers a broad range of applications. In particular, highly efficient and low-cost catalysts for pollutants degradation in wastewater and industrial effluents represent a challenging goal. Electrochemical advanced oxidation processes (EAOPs) [1–8], involving generation of very powerful oxidizing agents, such as, for instance, hydroxyl radical (•OH), have become especially relevant in wastewater treatment, particularly when the organic compounds present in solution are toxic or biorecalcitrant to conventional treatments. More recently, the electrochemical reduction of halogenated pollutants [9], by removing the halogen groups, has become an economic alternative to the EAOPs where the goal is the total organic mineralization. For this reason, the electrochemical reductive cleavage of carbon–halogen bonds in organic compounds, with the particular focus on volatile organic halides, has been mainly studied and developed in the last decades [10–13] being the subject of numerous studies in aqueous [14–16], non-aqueous [17–19] and mixed solvents [13,20]. The great interest for this process is due to its important role in some environmental applications, such as the abatement of volatile polychlorinated organic compounds, a group of pollutants having hazardous effects on living beings and out of the scope of most EAOPs.

The main core of the development of modern electrochemical systems is largely based on the use of nanostructured materials, since their electrocatalytic properties can be modulated through appropriate design and synthesis [21,22]. Moreover, their application to wide areas of environmental chemistry and energy conversion represents a field in constant growth [23–25]. Thus,

* Corresponding author at: Sorbonne Universités, UPMC Univ Paris 06, UMR 8235, Laboratoire Interfaces et Systèmes Electrochimiques, F-75005 Paris, France. Tel.: +33 1 44 27 41 58.
E-mail address: carlos.sanchez@upmc.fr (C.M. Sánchez-Sánchez).

http://dx.doi.org/10.1016/j.apcatb.2014.08.030
0926-3373/

electrocatalysis at nanoparticles represents one of the most exciting new frontiers in science, since it provides a very flexible and easy scalable methodology for potential industrial applications. In this context, the electrochemical dehalogenation of organic halides using nanostructured materials represents a very attractive and feasible alternative for working at mild reaction conditions and reduced costs [26,27]. As it is well documented in the literature, the process efficiency and the main reaction products depend on the electrode material, exhibiting silver the best electrocatalytic activity among all pure metals [9,10,28,29]. Furthermore, the electrocatalytic reduction of organic halides on silver has been already proved as a surface sensitive reaction, where the surface morphology must be considered as an important parameter for modulating the electrocatalytic effect [30]. Although most of the reported applications are performed on massive Ag electrodes, there are evidences [26,27,31,32] that micro- and nanostructured particles exhibit a better performance than massive silver, allowing a substantial reduction of Ag loading. For all these reasons, it is evident the great interest of studying the electrocatalytic properties of different types of silver nanoparticles (Ag NPs) in the degradation of halogenated pollutants. Moreover, the electrochemical dehalogenation of organic halides is an attractive reaction, not only for the mild reaction conditions, but also for the absence of additional reagents avoiding secondary pollution, which represents an important drawback in other decontamination treatments that may generate dangerous secondary reaction products [33].

The screening of electrocatalysts is a time-consuming task independently on the reaction of interest under scope. In this respect, trichloromethane electrochemical reduction is not different from other processes. Fortunately, new electroanalytical techniques have been recently introduced to improve this screening step. In particular, the scanning electrochemical microscopy (SECM) [34,35] has demonstrated its utility as a rapid and high-throughput technique in screening electrocatalyts [36] for processes such as the oxygen reduction reaction (ORR) [37–42], methanol interference during ORR [43], chlorine evolution [44] and oxygen evolution reactions (OER) [45,46], formic acid oxidation (FAOR) [47,48] and methanol oxidation reactions (MOR) [48]. Among the different modes of SECM, only the micropipette delivery/substrate collection (MD/SC) mode is based on non-electrochemically generated reactants and thus can be applied to study the trichloromethane reduction reaction [48]. The MD/SC mode is conceived for obtaining an electrocatalyst reactivity map by delivering the reactant of interest in the vicinity of an array formed by different electrocatalysts, while the array current is recorded and the micropipette is scanned on the *X*–*Y*-plane at a constant tip–substrate distance, as is schematically shown in Fig. 1. The rate of the species release is a function of its partition coefficient between two immiscible phases, being this species soluble in both of them, a water-immiscible organic solution within the pipette and an aqueous solution outside the pipette. The specific feature of the MD/SC approach lies on the possibility of dosing, in principle, any reactant, even if the latter cannot be electrogenerated (otherwise, the tip generation/substrate collection (TG/SC) mode represents a better choice). Thus, we herein extend the use of the MD/SC mode of the SECM for screening electrocatalysts for the trichloromethane electrochemical reduction reaction, since so far this mode was only used for studying MOR and FAOR. Note that in Fig. 1, but only for simplifying, we schematize the reaction at the substrate indicating the elimination of one single Cl^- per $CHCl_3$ molecule. But as a matter of fact, we know, from preparative electrolysis experiments reported in the literature using carbon-supported Ag NPs in aqueous solution [27], this reaction leads to a mixture of products, mostly formed by CH_4, which represents the complete dehalogenation (reaction (1)). However, using another electrocatalytic material and/or solvent, the reaction path and thus the product distribution may strongly vary. We present the SECM as a powerful technique that is able to observe the finest reaction rate differences at several catalysts under the same experimental conditions. To achieve this goal studying the trichloromethane electrochemical reduction, it is necessary to design a novel experimental setup, different from those already proposed previously in the literature. In fact, although the SECM has been already used for studying nano-sized materials as electrocatalysts [38,39], the current collector contribution to the total background current represents an important limitation on these systems, especially when the reaction of interest is close to the potential window limit, which is the case for the trichloromethane electrochemical reduction. For this reason, we introduce here a novel approach to reduce the current collector background contribution by using disposable screen-printed array electrodes [49]:

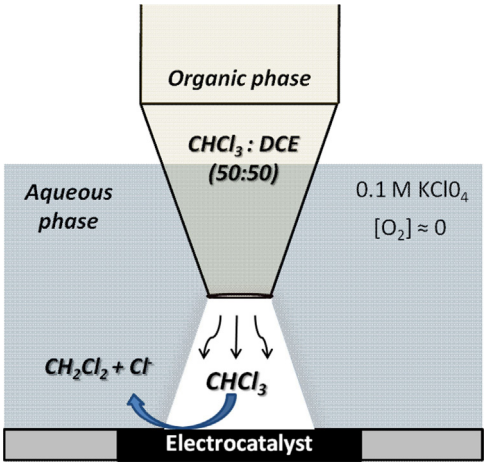

Fig. 1. Schematic representation of the MD/SC mode of the SECM applied to the screening of electrocatalysts for the $CHCl_3$ reduction reaction in aqueous medium.

$$CHCl_3 + 3H^+ + 6e^- \rightarrow CH_4 + 3Cl^- \quad (1)$$

In this work, we present the synthesis of three different sized Ag NPs used as electrode material for the reduction of a model volatile polychlorinated pollutant (trichloromethane, $CHCl_3$). The considered nanoparticles are prepared by simple colloidal methods, which represent a promising synthetic route for potential industrial scale preparation. The Ag NP activity is studied using two different methodologies: (i) A conventional study based on voltammetry and chronoamperometry, in which different batches of Ag NPs are supported on a glassy carbon (GC) electrode (almost inert material for this type of reaction [50]) and independently tested as catalyst for the reduction of $CHCl_3$ in aqueous solution. (ii) A novel screening approach based on the MD/SC mode of the SECM that allows for simultaneous analysis of different electrocatalysts under the same experimental conditions and provides rapid information about their activity and their resistance against deactivation. Finally, we also study the effect on the electrocatalysis of increasing the presence of defective sites (steps, kinks and high index planes) at the silver surface by following an electrochemical roughening protocol, using a bulky polycrystalline Ag electrode as a model.

2. Experimental

2.1. Chemicals

All chemicals were ACS reagent grade purchased from Sigma-Aldrich and were used without further purification. Trichloromethane ($CHCl_3$) anhydrous 99.8%, 1,2-dichloroethane

($CH_2Cl–CH_2Cl$, DCE) anhydrous 99.8%, potassium perchlorate ($KClO_4$) 99%, sodium borohydride ($NaBH_4$) 99%, trisodium citrate dihydrate 99%, silver nitrate ($AgNO_3$) 99%, octyltriethoxysilane 97.5%, sodium hydroxide (NaOH) (pellets) 98%, lead (II) perchlorate hydrate ($Pb(ClO_4)_2{\cdot}H_2O$) 99.995%. 100 μm diameter Ag wire (99.997% purity) was purchased from Alfa Aesar. All solutions were prepared with high-purity water obtained from a Millipore Milli-Q system with resistivity >18 MΩ cm at 25 °C.

2.2. Synthesis of silver nanoparticles (NPs)

Ag NPs studied here were synthesized using two different methodologies in order to produce different average size NPs: (i) sample (S1) was prepared using $NaBH_4$ as reducing agent following a well-established methodology for the synthesis of Au NPs [39,51,52], suitably modified for Ag NPs. Briefly, a 20 mL aqueous solution containing 2.5×10^{-4} M trisodium citrate dihydrate (which acts as stabilizer) and 1.25×10^{-4} M $AgNO_3$ (metallic precursor) was prepared in a conical flask at room temperature. Next, 0.6 mL of an ice-cold freshly prepared 0.1 M $NaBH_4$ solution was added to the solution under vigorous stirring. The stirring was slowed down after 30 s and for the next 15 min, the silver solution was stirred gently at room temperature to ensure removal of $NaBH_4$ excess. (ii) Samples (C1) and (C2) were prepared using trisodium citrate dihydrate as reducing agent following a procedure based on the Frens synthesis method [53] and adapted for obtaining Ag NPs. In particular, the $AgNO_3$ precursor was dissolved in water and heated under reflux conditions. After this, trisodium citrate was added and the solution was kept boiling for 30 min more, then quenched in an ice bath. Following this protocol, two different ratios of silver precursor/reducing agent were tested in order to synthesize different sized NPs. Sample C1 was synthesized by adding 0.8 mL of trisodium citrate 0.034 M and 100 mL of $AgNO_3$ 5×10^{-4} M solution. Sample C2 was synthesized by adding 3 mL of trisodium citrate 0.034 M and 100 mL of $AgNO_3$ 5×10^{-4} M solution.

The cleaning protocol necessary to remove organics attached to the NPs in all three samples (S1, C1 and C2), once the NPs were synthesized, comprised the addition of some NaOH pellets to each colloidal solution in order to break the colloid and precipitate the corresponding solid NPs. After complete precipitation, the samples were rinsed with water, at least 3–4 times, to make sure that clean aqueous NPs suspensions were obtained.

2.3. Physical characterization by TEM

Transmission electron microscopy (TEM) experiments were performed with a JEOL, JEM-2010 microscope working at 200 kV. The sample for TEM analysis was obtained by placing a drop of the dispersed suspension of NPs onto a Formvar-covered copper grid and evaporating the solvent in air at room temperature. TEM images of samples S1, C1 and C2 were obtained in two different stages of their synthesis and cleaning procedure. Firstly, one set of images were performed to the freshly prepared colloidal NPs and secondly, the same set of images were repeated for those NPs after complete precipitation and cleaning a few days later. For each sample, about 200–300 particles from different parts of the grid were used to estimate the mean diameter and size distribution of the NPs.

2.4. Electrochemical characterization of Ag NPs and a polycrystalline Ag electrode

2.4.1. Voltammetric and chronoamperometric studies

Cyclic voltammetry (CV) and chronoamperometry experiments were carried out in the same conventional electrochemical glass cell (solution volume = 50 mL) using a three-electrode configuration. The hemispherical polycrystalline Ag electrode (area = 0.095 cm^2) was prepared by melting an Ag wire until reaching an Ag bead. Then, the Ag bead was fixed to the bench in a random direction, cut in half and grinded with emery paper (600 grit) without further polishing. Before use, the hemispherical electrode was mechanically polished with different abrasive papers and alumina (0.05 μm) for reaching a mirror-like surface and sonicated in a water bath for 2 min before using it. The final radius of this hemispherical polycrystalline Ag electrode was measured by a Motic optical microscope (model DMBA200) connected with a built-in 3.0 megapixel camera. In contrast, each different type of Ag NPs (S1, C1 and C2) was independently deposited by dropcasting aliquots of 2 μL on a GC disc (4 mm diameter), allowing the water solvent to be evaporated in order to perform their electrochemical characterization. The aliquot volume of NPs was selected after the calibration procedure described in Section 2.4.2. Before each new experiment, the GC disc was mechanically polished with 0.05 μm alumina, sonicated and rinsed with water to eliminate the particles from previous experiments. The counter and the reference electrodes were a gold wire (0.5 mm diameter) and a saturated calomel electrode (SCE), respectively. All measurements were made using a computer-controlled Autolab PGSTAT30 potentiostat driven by NOVA software. The only difference between CV and chronoamperometry in the experimental setup was the magnetic stirring, which was exclusively used during chronoamperometric measurements.

2.4.2. Calibration of Ag NPs loading

The calibration procedure described in this paragraph aims to main goals: (i) decoupling the role of the specific surface area (i.e. the catalytic surface area available per volume unit of NPs suspension, in this case expressed as $cm^2\ \mu L^{-1}$) and (ii) determining the correct loading range in which the whole ensemble of NPs deposited onto the GC are available and participate into the faradaic process of interest without any diffusion limitation. In order to achieve these goals, the lead underpotential deposition (Pb UPD) represents the most convenient and adopted method used for calibrating Ag-based electrodes [54,55].

In this work, the specific surface area of each type of Ag NPs was electrochemically determined using the charge involved in the Pb UPD region of the corresponding CV that takes place within the range −0.2 and −0.8 V vs. SCE in a 0.1 M NaOH and 5×10^{-3} M $Pb(ClO_4)_2$ deaerated solution at scan rate 10 mV s^{-1}. For this process, we adopted the calibration charge density value reported in the literature for a polyoriented silver electrode, which is 280 $\mu C\ cm^{-2}$ [54,55]. Thus, the initial surface area of all three Ag NP samples determined by Pb UPD was 0.0025 $cm^2\ \mu L^{-1}$ for sample S1, 0.0056 $cm^2\ \mu L^{-1}$ for C1 and 0.0090 $cm^2\ \mu L^{-1}$ for C2. A typical Pb UPD CV on Ag NPs (sample S1) is reported in Fig. 2A, which includes a dashed line limiting the double-layer contribution and perfectly defining the cathodic current integration region corresponding to the Pb UPD. Fig. 2B (for sample S1) displays the correlation between the trichloromethane reduction current coming from the CVs provided by different aliquots of Ag NPs S1 (from 1 to 10 μL) and their corresponding specific surface area calculated from Pb UPD calibration. Thus, the linear loading range in which the whole ensemble of Ag NPs deposited onto GC do not present diffusion limitations shown in Fig. 2B corresponds to Ag NPs aliquots between 1 and 2.5 μL, which ranges from 0.0025 to 0.0062 cm^2 (delimited by a dashed line in Fig. 2B) of total Ag surface exposed. Further increase of Ag loading does not lead to a proportional increase of trichloromethane reduction current, most likely due to diffusion limitations in the inner part of the Ag deposit. This limitation is also observed in Ag NPs C1 and C2, since they were both diluted to reach an initial surface area of 0.0025 $cm^2\ \mu L^{-1}$. For this reason, 2 μL is the selected loading used for evaluating all three Ag NP samples performance for trichloromethane reduction

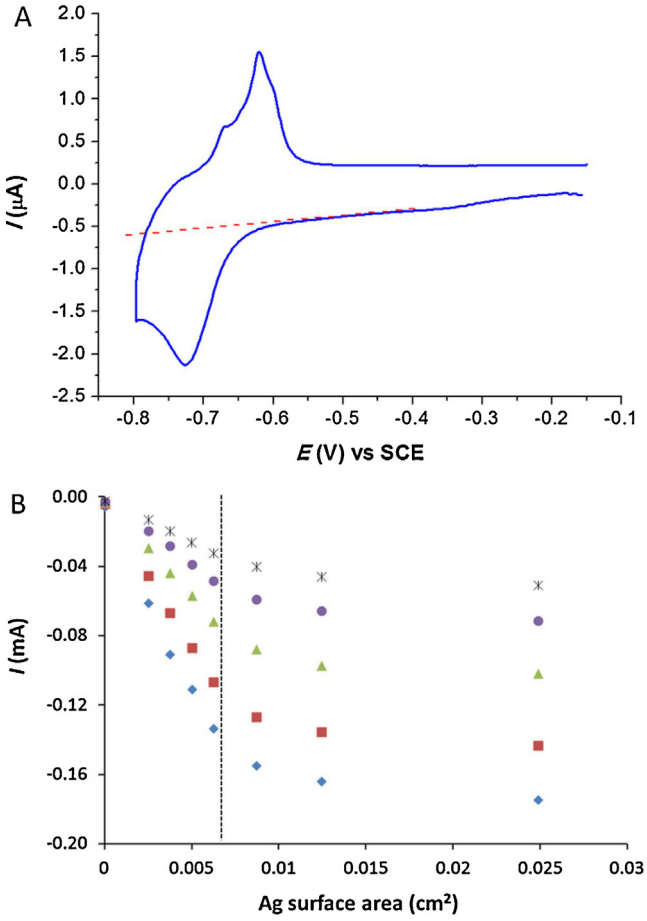

Fig. 2. (A) Voltammetric profile at the Pb UPD region of 7 μL of Ag NPs suspension (sample S1) in 0.1 M NaOH + 5×10^{-3} M $Pb(ClO_4)_2$ deaerated solution. Scan rate 10 mV s^{-1}. (B) Relationship between the trichloromethane reduction current at different applied potentials provided by different aliquots of Ag NPs S1 (from 1 to 10 μL) and their corresponding specific surface area determined by Pb UPD. Applied potentials: −0.9 V (black starts), −0.95 V (purple circles), −1.0 V (green triangles), −1.1 V (red squares) and −1.2 V (blue rhombus).

by CV. In contrast, Ag NP samples studied by SECM were normalized by solvent evaporation, to obtain three new aqueous suspensions with different NP concentration, but equal specific Ag surface area (0.017 cm^2 μL^{-1}).

2.4.3. Catalytic activity of Ag NPs and a polycrystalline Ag electrode in $CHCl_3$ solution

The potential range scanned by CV was from −0.2 to −1.2 V at a scan rate of 50 mV s^{-1}. The constant potential applied during the chronoamperometries was −1.2 V. Magnetic stirring and constant gas bubbling were exclusively used during the chronoamperometric measurements. All current densities (j, mA cm^{-2}) reported herein were calculated using the real surface area determined by Pb UPD and not the geometric area of the corresponding electrode. In all cases, the electrolyte was a freshly prepared aqueous solution containing 0.1 M $KClO_4$ and 0.01 M $CHCl_3$ purged with N_2 for at least 15 min before the experiment. Solutions were homogeneous since the $CHCl_3$ maximum solubility in water reported at 20 °C is 8 g/L (0.067 M) [56], which is significantly higher value than the concentration used here. Due to the high volatility of $CHCl_3$, the N_2 gas used for purging was previously saturated by flowing through another solution with equal composition to avoid any change in the $CHCl_3$ concentration during the cyclic voltammetries and chronoamperometries.

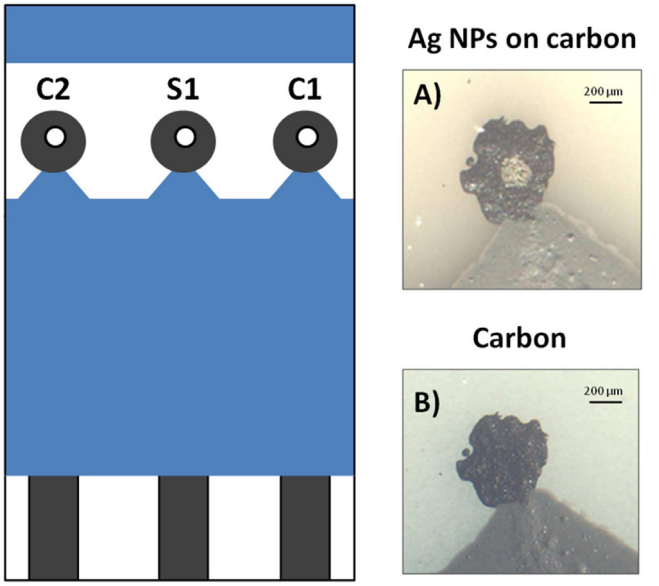

Fig. 3. Schematic representation of a disposable screen-printed linear carbon array electrode including the three Ag NP samples studied (S1, C1 and C2). Optical microscope photos of one of the carbon disc belonging to the screen-printed carbon array electrode with (A) and without (B) the Ag NPs dispensed on top.

2.5. Preparation of an array of Ag NPs using disposable screen-printed array electrodes

A picoliter solution dispenser (CHI 1550, Austin, TX) was used to dispense the three types of Ag NPs dispersed in water on a commercial disposable screen-printed linear carbon array electrode (product code: KRS-1004 from Kanichi Co.) used as a platform and schematically reported in Fig. 3. This type of electrodes was selected as an appropriate platform to minimize the background current coming from the carbon current collector. They are built on a polyester substrate by printing a carbon ink pattern of controlled dimensions, which defines the electrode geometry (three disc electrodes of 570 ± 5 μm diameter), and a dielectric paste for masking the connections from solution. This configuration causes a difference in height between the carbon electrode surface and the dielectric, being the former 10 μm higher than the latter. Then, each one of the three different suspensions of Ag NPs (S1, C1 and C2) was dispensed at the center of one of the carbon disc electrodes. Each Ag NP suspension was sonicated for 2 min before charging the dispenser in order to ensure their homogeneity. Then, a total of 200 drops of each Ag NP suspension were dispensed in each spot in 10 sets of 20 drops each, allowing the water solvent to be evaporated before each new set of drops was added. The volume of each drop dispensed by the CHI 1550A is within the range 100–200 pL and it will vary within that range depending on the potential applied into the piezoelectric jetting device (50 V in this case). The final diameter size of all three Ag NP spots on the carbon disc electrodes were 190 ± 5 μm and they were 2200 μm apart. All these size values were measured by a Motic optical microscope (model DMBA200) connected with a built-in 3.0 megapixel camera.

2.6. Micropipette fabrication

Micropipettes with a reproducible opening diameter were fabricated by pulling borosilicate capillaries with an O.D. of 2.0 mm, an I.D. of 1.0 mm and length of 90 mm using a laser-based puller P-2000 from Sutter Instrument Co. The diameter was measured using an optical microscope DMBA200 from Motic Co. The inner walls of the micropipettes were made hydrophobic following a

well-established silanization protocol [57,58] by filling them with octyltriethoxylsilane overnight and finally, drying them exhaustively.

2.7. Scanning electrochemical microscopy (SECM)

All SECM images were carried out using the MD/SC mode of SECM in a CHI 910B microscope (CH Instruments) and a three-electrode configuration at room temperature. The micropipettes used to deliver the $CHCl_3$ in the vicinity of the substrate electrodes presented a diameter of 40 μm and were loaded either with a mixture 50:50 $CHCl_3$:DCE (v/v) or only DCE for the blank experiments. A commercial SCE electrode within a Luggin capillary was used as reference and a gold wire, 0.5 mm diameter, as counter-electrode in all SECM experiments.

a) *SECM MD/SC imaging of an Ag 100 μm substrate.* A 100 μm diameter Ag ultramicroelectrode (UME) was employed as a substrate electrode for collecting, by electrochemical reduction, the $CHCl_3$ delivered by the micropipette. This electrode was built by heat-sealing, under vacuum, a silver wire in a flint glass capillary [34]. After this, the capillary glass was polished using sand paper and alumina powders (0.3 and 0.05 μm) to yield a flat disc and to reveal the silver surface. The usual parameters to define this type of electrodes are the tip radius (a), the tip radius including the glass sheath (rg), the RG value ($RG = rg/a$), and for positioning them, the normalized distance ($L = d/a$), where d is the tip–substrate distance along the Z-axis. The silver electrode used for the SECM imaging presented $a = 50$ μm and $RG = 20$. The electrochemical cell employed was built in Teflon with a 2 mm diameter aperture, where the Ag UME perfectly fitted facing up and was held at a potential value negative enough to produce the electrochemical reduction of $CHCl_3$ at its surface. The micropipette was located at a constant tip–substrate distance in Z ($d = 50$ μm) facing the Ag UME and the MD/SC images were obtained recording the substrate current while the micropipette was scanned on the X–Y-plane in an oxygen-free 0.1 M $KClO_4$ solution. The tip scan rate was 25 μm s^{-1}.

b) *SECM MD/SC imaging of an array of Ag NPs.* A disposable screen-printed linear carbon array electrode in which the three Ag NPs samples (S1, C1 and C2) were previously deposited was used as a substrate electrode. The electrochemical cell employed was built in Teflon with an 8 mm diameter aperture, where the substrate electrode was tightened via an O-ring, allowing the three Ag NP samples contacting the 0.1 M $KClO_4$ solution. Before imaging, removal of the substrate tilt is required. For that purpose, a conventional 25 μm diameter Au UME ($RG = 3$) was used instead of the micropipette and successive negative feedback approach curves were performed at −0.8 V using the O_2 in solution as a redox mediator until the tilt correction reached $\Delta z/\Delta x$ (or Δy) ≤ 1.5 μm/mm. That UME tip was built by heat sealing under vacuum a gold wire in a flint glass capillary as described above for the Ag UME. After tilt correction, the Au UME was substituted by the micropipette, which was carefully approached in physical contact with the substrate and then withdrawn 50 μm in the Z-direction. The 0.1 M $KClO_4$ solution was deaerated with Ar and a gas blanket was maintained over during the experiment to keep the solution free from atmospheric oxygen. For each SECM image, the substrate potential of all three addressable electrodes was held constant in an active region for the $CHCl_3$ reduction reaction on silver. Then, an SECM image represents a reactivity map by displaying the $CHCl_3$ reduction current produced at the substrate when the micropipette delivers $CHCl_3$ and is scanned in the X–Y-plane above the different Ag NPs as a function of tip position. The protocol after each SECM image to restore the electrocatalysts to their initial conditions consists in bubbling argon within the solution while the substrate potential is held at -1.3 V during 300 s to clean the electrode surface from reactant adsorption. The tip scan rate was 100 μm s^{-1}, using increments of 20 μm each 0.2 s.

2.8. Electrochemical roughening of a polycrystalline Ag electrode

The roughness factor (Rf) corresponds to the ratio between real surface area and geometric area at the electrode. For a proper evaluation of this parameter, it is necessary to perform the Pb UPD to the polycrystalline Ag electrode and compare this with its geometric area. Initially, this electrode presented a Rf = 1.72, since its surface was smoothed by polishing. But it is possible to perform and electrochemical roughening (ER) protocol that should allow increasing the real surface area keeping constant the geometric area. For that purpose, the polycrystalline Ag electrode underwent three consecutive oxidation–reduction cycles between +0.26 V (silver dissolution) and −1.3 V (silver redeposit) in a 0.1 M $KClO_4$ deaerated solution by consecutively stepping the electrode potential between those two limits. This procedure only generates short terraces and an important increase in the step and kink sites at the electrode surface. The time-length of each potential step was calculated in order to reach the oxidation (and the subsequent reduction) of less than one monolayer of silver atoms at the electrode surface. Following this protocol and varying the total charge employed, we prepared two different electrodes: Ag ER1 with an Rf = 1.97 (charge equivalent to one-third of a monolayer, 53 μC) and Ag ER2 with an Rf = 2.02 (charge equivalent to one full monolayer, 157 μC). After this, the Ag electrode was rinsed with water and immediately immersed in the electrochemical cell containing trichloromethane for CV analysis, carried out as described in Section 2.4.3.

3. Results and discussion

As expected, the three different samples of Ag NPs synthesized and studied here present, despite the presence of some nanorods, a preferential quasi-spherical shape, which is generally assigned to a polyoriented and non-specifically structured catalyst surface. In addition, the different protocols of synthesis employed here produce NPs with different average sizes. In fact, it is known from literature [59,60] that the smallest NPs are obtained using the most powerful reducing agent ($NaBH_4$) and larger NPs are synthesized by using citrate as reducing agent. Fig. 4 shows the TEM images corresponding to the freshly prepared colloidal suspensions of Ag NPs (4A, 4B and 4C) and corroborates that the S1 sample presents the smallest average particle size among the three samples studied (about 6 nm). On the other hand, C1 sample exhibits the largest average particle size (about 50 nm) and C2 sample shows a bimodal distribution with medium-sized spherical NPs (40 nm) and long nanorods. A relevant aspect for studying electrocatalysis on NPs is the cleaning protocol performed after the NPs have been synthesized to ensure the use of clean (organics free) Ag NPs. Unfortunately, clean Ag NPs in aqueous suspension do not remain invariant in size and the effect of light exposition and changes in storage temperature provoke the catalyst particles growth with time. This is mainly due to the dissolution of small Ag NPs and their subsequent re-deposition forming larger NPs, which are thermodynamically more favorable (Ostwald ripening). Thus, Fig. 4D–F shows the enlargement of Ag NPs produced in all three samples with time (after a few days of storage in aqueous suspensions) and the agglomeration of long Ag nanorods in sample C2 (300 nm long, Fig. 4F). For that reason and in order to avoid any distortion in the Ag samples specific area quantification, this is determined by means of Pb UPD with a short delay with respect to either the voltammetric,

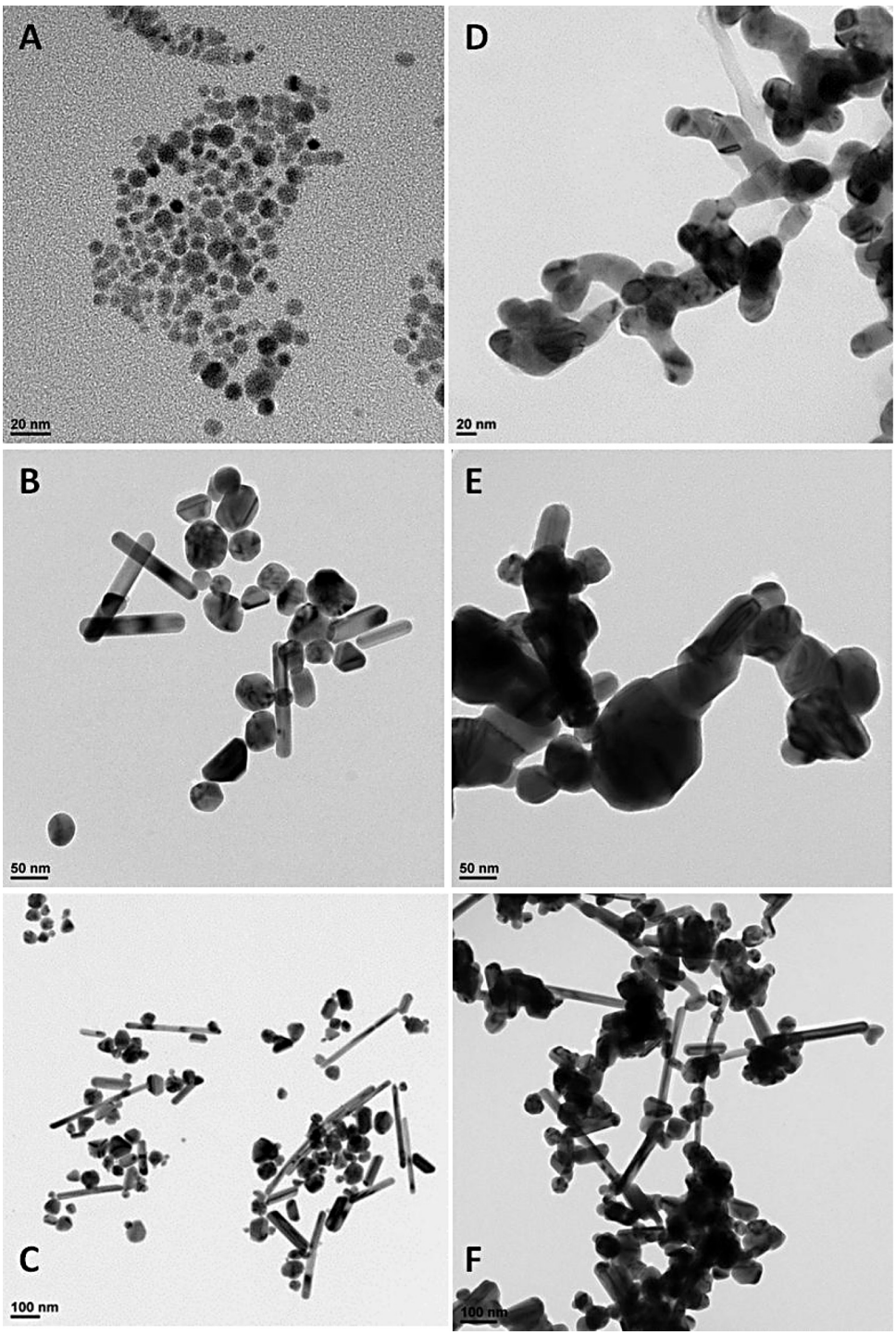

Fig. 4. TEM pictures of the three different Ag NPs synthesized. (A–C) Freshly prepared colloidal samples S1, C1 and C2, respectively, and (D–F) clean Ag NPs in aqueous suspension S1, C1 and C2, respectively, after several days of storage. Only samples D–F are electrochemically characterized and studied.

chronoamperometric or SECM experiments. In all those cases, only clean Ag NPs are studied (Fig. 4D–F).

Initially, the catalytic activity of the three different types of Ag NPs synthesized is evaluated using conventional electrochemical techniques, CV to estimate their instantaneous activity and chronoamperometry to provide their long-term performance activity. Fig. 5A depicts the cyclic voltammograms corresponding to the three different Ag NP samples in the presence and in the absence (background) of $CHCl_3$. A clear reduction current increase is observed between −0.8 and −1.2 V associated to the electrochemical reduction of the $CHCl_3$ present in solution. It is worthwhile to remind that in Fig. 5 the current density values displayed are obtained considering the real specific area for each type of NPs as determined by the Pb UPD analysis described in Section 2.4.2. This means that the results reported in Fig. 5A represent a direct evaluation of the reaction rate at each material. In order to provide a fair comparison among the instantaneous activity of samples S1, C1 and C2, the current density values at different potentials are estimated from their corresponding voltammograms and are displayed in Fig. 5B. This comparison shows that samples S1 and C1 show the highest current at high overpotential (−1.2 V) and sample C2 shows the highest current at low overpotential (−1.0, −0.9 and

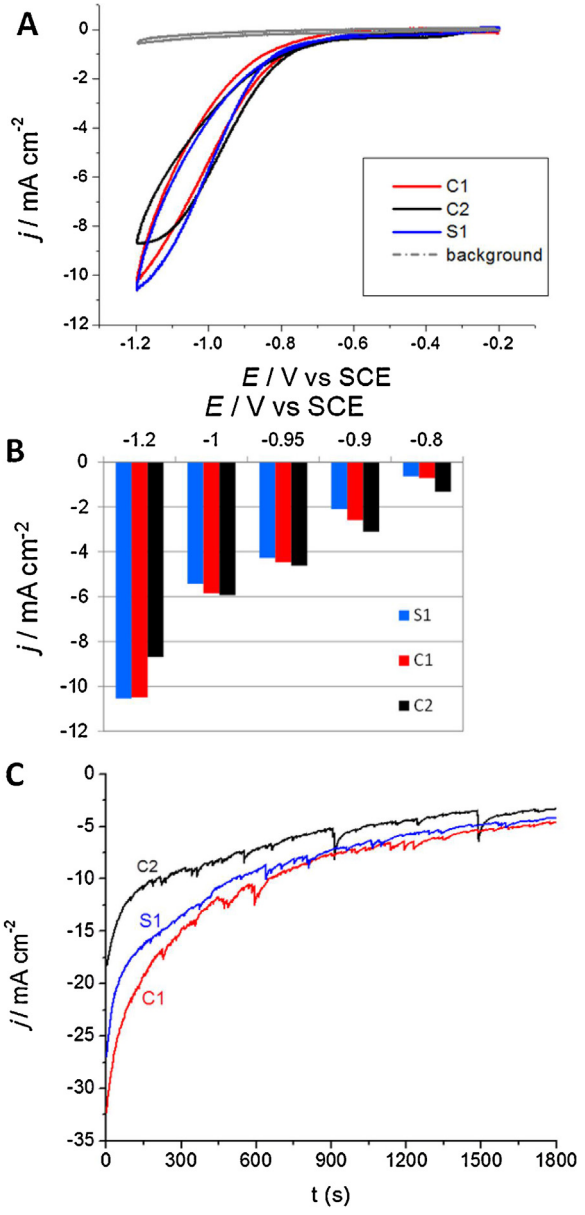

Fig. 5. Catalytic evaluation of the three different Ag NP samples: S1 (blue plot), C1 (red plot) and C2 (black plot) in a 0.1 M $KClO_4$ and 0.01 M $CHCl_3$ deaerated solution by CV and chronoamperometry. (A) Voltammetric profiles in the presence and absence (background) of $CHCl_3$ in solution. Scan rate 50 mV s^{-1}. (B) Instantaneous catalytic activity obtained from their corresponding voltammograms (A). (C) Chronoamperometries at −1.2 V meanwhile the solution is stirred.

−0.8 V) as is clearly shown in Fig. 5B. Therefore, we can propose that C2 is the most intrinsically active material, since it shows the highest current density values at potentials at which charge-transfer kinetics plays a role. On the other side, to correctly interpret the improved behavior of C1 and S1 at the most negative potentials, it should be taken into account that the electroreduction of organic polyhalides on an active surface is always a complex combination of phenomena that can lead to (i) a superimposition of different peaks, each relevant to a different type of surface site or different steps in the reaction mechanism (removal of the 1st, 2nd or 3rd chloride) [32] and (ii) the co-presence of adsorption- and diffusion-limited peaks [61]. In parallel, we could also propose a more rapid deactivation of C2 sites than S1 and C1. This process might be controlled by the presence of a high concentration of chloride only reached at high overpotentials. Notwithstanding, it is not the purpose of this work to further investigate the reaction path or undergo a deeper CV analysis. Thus, we consider C1 and S1 as the most promising electrode materials in view of practical applications, because of their high reaction rates under pollutant degradation operative conditions. To further gain insights on these material features, we evaluate their long-term stability in electrolysis at constant potential. Fig. 5C shows the corresponding chronoamperometries performed at −1.2 V for 30 min for all three Ag NP samples. The results point to the fact that although all three Ag NP samples undergo a deactivation process in long-term electrolyses, C1 shows the highest current. Then, it is important to highlight again that instantaneous performance obtained from CV is not always enough to evaluate the real performance of an electrode material, since the contribution from the electrode deactivation processes may be hindered and not taken into account.

In addition, the catalytic activity of the three different types of Ag NPs synthesized is evaluated using the SECM. In order to do this, first of all it is necessary to demonstrate the feasibility of this technique for studying the $CHCl_3$ reduction reaction. For this purpose, a disc-shaped Ag 100 μm UME is used as a model substrate electrode, since it does not present additional background contributions. Fig. 6 shows three different SECM MD/SC images displaying a color code for representing the different current collected at the Ag UME substrate, while the micropipette scans its surface. The current intensity map shown in these SECM images displays dark green and brown areas corresponding to low and high currents collected on the substrate electrode, respectively. If the micropipette is filled with a mixture 50:50 (v/v) DCE:$CHCl_3$, then $CHCl_3$ goes out of the micropipette by crossing the liquid–liquid interface and is easily collected by the Ag substrate electrode, which is held at a proper potential. Fig. 6A and B clearly exhibits a central region where the $CHCl_3$ reduction current increases, which corresponds with the presence of the Ag electrode. Furthermore, the current collected at the substrate is higher at −1.2 V (Fig. 6B) than at −1.0 V (Fig. 6A), following the same behaviour displayed at Fig. 5. Finally, Fig. 6C displays a blank experiment, since the micropipette is only filled with DCE and thus, only a negligible current is collected when this micropipette scans the Ag electrode surface. For this reason, the SECM image in Fig. 6C displays one single color, since all current values represented there are included within the background (current range within the image at Fig. 6C, from −2.48 to -3.17×10^{-8} A). This blank experiment rules out any possible competition in the dehalogenation reaction on silver coming from the DCE (a molecule that could, in principle, be a competitor for electroreduction [15]). Therefore, it is demonstrated that SECM is a valid technique to evaluate the activity for the $CHCl_3$ reduction reaction at the three different types of Ag NPs synthesized. At this point, it is important to note that for being able to compare simultaneously by SECM the activity of the different Ag NPs under the same conditions, it is necessary to use the same surface area in each sample deposited on the disposable screen-printed array electrode. Then, an evident color difference in the SECM image would be univocally associated with a higher reaction rate for the $CHCl_3$ reduction. Fig. 7 shows the SECM MD/SC image comparing all three Ag NPs samples (S1, C1 and C2) at −1.2 V, the potential that could be adopted in practical environmental applications. The activity shown by this SECM MD/SC image is independent of Ag specific surface area, since they are all equal. Thus, the most promising Ag catalyst sample is C1 because it displays the highest reduction current (brown color) therein. In contrast, samples S1 and C2 present lower currents but comparable among them, being a bit higher for S1. Thus, the ranking given by this rapid SECM screening is C1 > S1 > C2, following the exactly same trend already found using chronoamperometry (Fig. 5C), but in this case using only one single experiment performed under identical experimental conditions. The fact that a little trail appears in Fig. 7 can be associated with the fact that not all the $CHCl_3$ released from

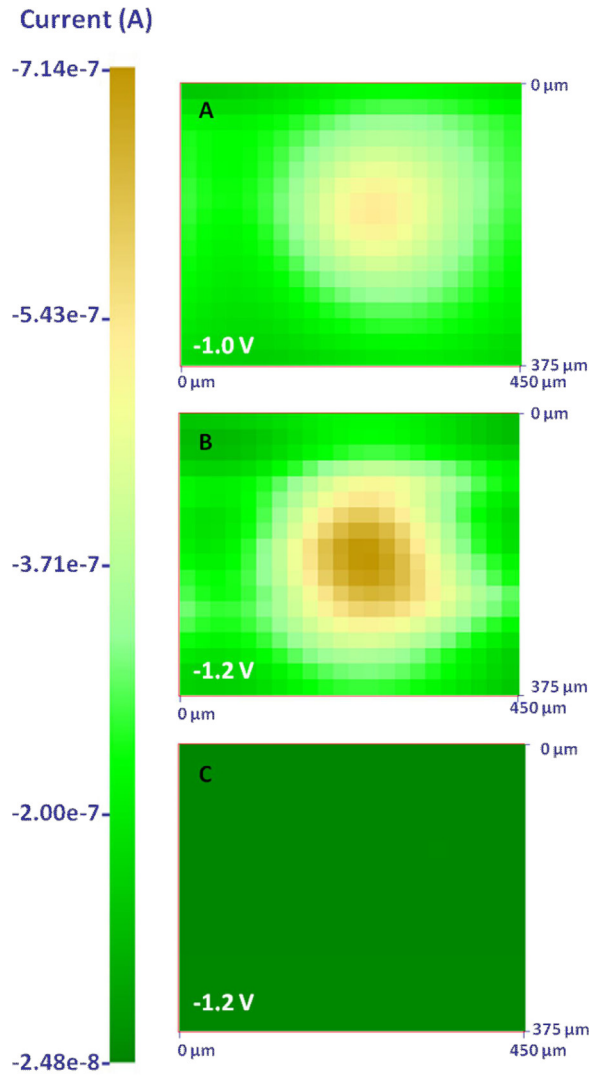

Fig. 6. SECM MD/SC images displaying the current collected for $CHCl_3$ reduction in 0.1 M $KClO_4$ solution at a 100 µm Ag UME. The tip scan rate was 25 µm s^{-1} and the pipette–substrate distance was 50 µm. Micropipette filled with 50:50 (v/v) DCE:$CHCl_3$ and potential applied at the Ag UME substrate −1.0 V (A) and −1.2 V (B). Micropipette filled only with DCE and potential applied at the Ag UME substrate −1.2 V (C).

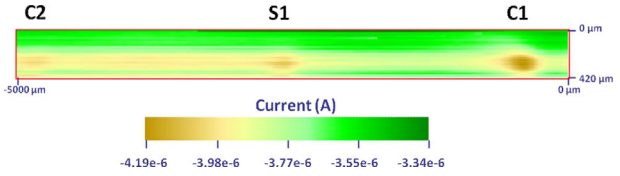

Fig. 7. SECM MD/SC image displaying the substrate current for $CHCl_3$ reduction of an array composed by three different types of Ag NPs supported on a disposable screen-printed linear carbon array electrode. Substrate potential held constant at −1.2 V in an oxygen-free 0.1 M $KClO_4$ solution. Tip–substrate distance = 50 µm. The tip scan rate was 100 µm s^{-1}, using increments of 20 µm each 0.2 s.

the micropipette is instantaneously consumed at the Ag samples S1 and C2, but it is mainly done at sample C1. For this reason, it is possible to continue electroreducing some of the $CHCl_3$ accumulated in solution and not previously consumed, even when the micropipette is located far away from the Ag NPs samples, reporting in this way a reduction current decoupled from the micropipette location and giving as a result the formation of a trail within the SECM image. We believe that this kind of artifact does not represent a severe

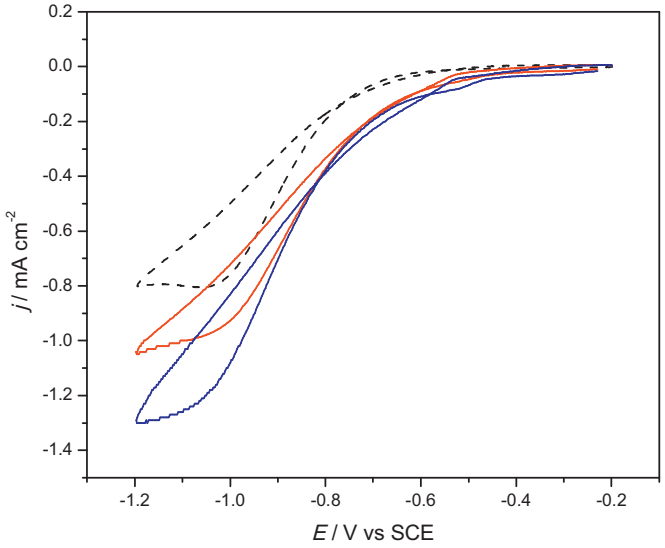

Fig. 8. Voltammetric response of a polycrystalline Ag electrode before (dashed black plot, Rf = 1.72) and after the electrochemical roughening treatment, Ag ER1 (red plot, Rf = 1.97) and Ag ER2 (blue plot, Rf = 2.02). Specific surface areas determined by Pb UPD. Deaerated solution composition 0.1 M $KClO_4$ and 0.01 M $CHCl_3$. Scan rate 50 mV s^{-1}.

limitation to validate this screening method. On the contrary, we safely propose the rapid screening method described so far as a high sensitivity tool to quickly characterize NPs performance.

In order to explain the different reactivity exhibited here by the three types of Ag NPs, which has been confirmed by both techniques, chronoamperometry and SECM, it is necessary to pay attention to the differences in size and surface structure present in all three samples. It is well established in the literature [30,62,63] that a significant increase in the silver electrocatalytic effect is observed when a high density of defective sites (steps, kinks and high index planes) are generated by following an electrochemical roughening protocol at the silver surface. In contrast, long terraces mainly free of steps and kinks present a less active catalytic effect. Consequently, it seems reasonable that, due to a higher abundance of long nanorods in which large terraces should be present, Ag NPs C2 present the lowest percentage of defective sites at their surface. On the other hand, Ag NP C1 exhibits higher current densities than Ag NP S1 because its average particle size is much bigger. This larger amount of surface atoms available allows for the presence of high index planes, which are barely possible in small size NPs. For these reasons, and despite Ag NP C1 does not possess the best intrinsic activity (that belongs to Ag NP C2), they present a large amount of defective sites for which the balance between activity and deactivation rates lead to the best overall catalytic performance under pollutant degradation conditions. In order to validate this hypothesis, the effect of the electrochemical roughening on a massive, polycrystalline Ag electrode for the trichloromethane electrochemical reduction is also studied. Fig. 8 shows the corresponding CVs for the polycrystalline Ag electrode after undergoing the roughening treatment in different extension (ER1, 53 µC (Rf = 1.97) and ER2, 157 µC (Rf = 2.02)) and without any treatment (blank). In all three cases, the current values reported are normalized with respect to their real Ag surface areas measured by Pb UPD. These voltammograms show the increase in the reduction current densities for both roughened Ag electrodes with respect to the untreated electrode and point to a significant and beneficial effect of surface disorder by increasing the concentration of step and kink sites. This is clearly demonstrated by the positive shift of the onset potential (formation of new, active sites) and the increase in current densities

in the whole potential window, indicating a general improvement of reactivity performances.

4. Conclusions

The use of the SECM as a powerful catalysts screening tool in electrochemical reactions is proved for the first time useful for an environmental application. This electrocatalyst screening is performed by simultaneously comparing three different Ag NPs samples under constant experimental conditions. In particular, this is tested for the electrochemical degradation of a model volatile polychlorinated organic compound, such as $CHCl_3$, in aqueous electrolyte. This cathodic detoxification treatment allows to selectively produce less chlorinated compounds by hydrodehalogenation in aqueous medium, directly treating the contaminated water without including any further separation process. All Ag NPs synthesized for this work, prepared using a low-cost scalable method, are only studied after removing organics from their surface, despite that provokes catalyst NPs growth and agglomeration. In all three cases, they exhibit high performances, comparable with the most promising materials presented in the literature so far.

The performance ranking obtained by the SECM for the three different samples of Ag NPs synthesized is C1 > S1 > C2. The ranking is established after the role of secondary effects such as the specific Ag surface area of each sample is normalized for a proper comparison. This activity trend is validated by its comparison with the results obtained by conventional electrochemical techniques such as chronoamperometry, which demonstrates the feasibility and the good sensitivity of SECM in electrocatalyst screening for the $CHCl_3$ reduction reaction in aqueous medium. We propose the proper size range and the presence of abundant defective sites, such as steps or kinks, as the main reasons for Ag NPs C1 exhibiting the best overall catalytic performance in trichloromethane electrochemical reduction. Furthermore, we herein introduce the novel use of disposable screen-printed array electrodes as proper substrate electrodes for studying nanomaterials by SECM with a negligible background current contribution.

The MD/SC mode of the SECM based on the use of micropipettes for delivering the species of interest in the proximity of the electrocatalyst allows to increase the scope of this screening technique to non-electrochemically generated species, such as $CHCl_3$, which is used here as a model molecule to prove the concept. Nevertheless, we think that other interesting halogenated molecules from an environmental point of view should be affordable using the same methodology. In conclusion, this type of SECM screenings allows to analyze a large number of samples in one single experiment under the same experimental conditions, since this is only limited by the number of available carbon electrodes present in the disposable screen-printed array electrode in contact with the test solution.

Acknowledgements

This work has been partially financed by the MICINN (Spain) (project CTQ2010-16271) and Generalitat Valenciana (projects PROMETEO/2009/045271 and GRISOLIA/2011/029). O.L. is thankful to Università degli Studi di Milano for his Ph.D. fellowship.

References

[1] B.P. Chaplin, Environ. Sci.: Processes Impact 16 (2014) 1182–1203.
[2] L. Feng, E.D. van Hullebusch, M.A. Rodrigo, G. Esposito, M.A. Oturan, Chem. Eng. J. 228 (2013) 944–964.
[3] E. Brillas, I. Sirés, M.A. Oturan, Chem. Rev. 109 (2009) 6570–6631.
[4] A. Thiam, M. Zhou, E. Brillas, I. Sires, Appl. Catal. B 150–151 (2014) 116–125.
[5] M. Panizza, G. Cerisola, Chem. Rev. 109 (2009) 6541–6569.
[6] B. Marselli, J. Garcia-Gomez, P.A. Michaud, M.A. Rodrigo, C. Comninellis, J. Electrochem. Soc. 150 (2003) D79–D83.
[7] K. Rajeshwar, J.G. Ibañez, Environmental Electrochemistry Fundamentals and Applications in Pollution Abatement, Academic Press, San Diego, CA, 1997.
[8] M. Villanueva-Rodriguez, C.M. Sánchez-Sánchez, V. Montiel, E. Brillas, J.M. Peralta-Hernandez, A. Hernandez-Ramirez, Electrochim. Acta 64 (2012) 196–204.
[9] S. Rondinini, A. Vertova, in: C. Comninellis, G. Chen (Eds.), Electrochemistry for the Environment, Springer, Berlin, 2010 (Chapter 12).
[10] S. Rondinini, P.R. Mussini, P. Muttini, G. Sello, Electrochim. Acta 46 (2001) 3245–3258.
[11] S. Rondinini, P.R. Mussini, P. Specchia, A. Vertova, J. Electrochem. Soc. 148 (2001) D102–D107.
[12] S. Rondinini, A. Vertova, Electrochim. Acta 49 (2004) 4035–4046.
[13] G. Fiori, S. Rondinini, G. Sello, A. Vertova, M. Cirja, L. Conti, J. Appl. Electrochem. 35 (2005) 363–368.
[14] Y.H. Xu, H. Zhang, C.P. Chu, C.A. Ma, J. Electroanal. Chem. 664 (2012) 39–45.
[15] O. Scialdone, C. Guarisco, A. Galia, R. Herbois, J. Electroanal. Chem. 641 (2010) 14–22.
[16] Y.H. Xu, Q.Q. Cai, H.X. Ma, Y. He, H. Zhang, C.A. Ma, Electrochim. Acta 96 (2013) 90–96.
[17] A.A. Isse, B.B. Huang, C. Durante, A. Gennaro, Appl. Catal. B 126 (2012) 347–354.
[18] C. Durante, A.A. Isse, G. Sandona, A. Gennaro, Appl. Catal. B 88 (2009) 479–489.
[19] A.A. Isse, G. Sandona, C. Durante, A. Gennaro, Electrochim. Acta 54 (2009) 3235–3243.
[20] Y. Hori, K. Murata, T. Oku, Chem. Lett. 32 (2003) 230–231.
[21] S.E.F. Kleijn, S.C.S. Lai, M.T.M. Koper, P.R. Unwin, Angew. Chem. Int. Ed. 53 (2014) 3558–3586.
[22] R.W. Murray, Chem. Rev. 108 (2008) 2688–2720.
[23] E.J.E. Stuart, K. Tschulik, D. Omanovic, J.T. Cullen, K. Jurkschat, A. Crossley, R.G. Compton, Nanotechnology 24 (2013) 444002.
[24] M.K. Debe, Nature 486 (2012) 43–51.
[25] I. Katsounaros, S. Cherevko, A.R. Zeradjanin, K.J.J. Mayrhofer, Angew. Chem. Int. Ed. 53 (2014) 102–121.
[26] A. Minguzzi, O. Lugaresi, G. Aricci, S. Rondinini, A. Vertova, Electrochem. Commun. 22 (2012) 25–28.
[27] S. Rondinini, G. Aricci, Z. Krpetic, C. Locatelli, A. Minguzzi, F. Porta, A. Vertova, Fuel Cells 9 (2009) 253–263.
[28] B. Huang, A.A. Isse, C. Durante, C. Wei, A. Gennaro, Electrochim. Acta 70 (2012) 50–61.
[29] A. Gennaro, C.M. Sánchez-Sánchez, A.A. Isse, V. Montiel, Electrochem. Commun. 6 (2004) 627–631.
[30] S. Ardizzone, G. Cappelletti, L.M. Doubova, P.R. Mussini, S.M. Passeri, S. Rondinini, Electrochim. Acta 48 (2003) 3789–3796.
[31] A.A. Isse, S. Gottardello, C. Maccato, A. Gennaro, Electrochem. Commun. 8 (2006) 1707–1712.
[32] A. Vertova, R. Barhdadi, C. Cachet-Vivier, C. Locatelli, A. Minguzzi, J.-Y. Nedelec, S. Rondinini, J. Appl. Electrochem. 38 (2008) 965–971.
[33] S. Rondinini, A. Minguzzi, A. Vertova, in: G. Kreysa, K. Ota, R.F. Savinell (Eds.), Encyclopedia of Applied Electrochemistry, Springer Reference, 2014, pp. 1398–1402.
[34] A.J. Bard, M.V. Mirkin (Eds.), Scanning Electrochemical Microscopy, Marcel Dekker, New York, 2001.
[35] M.V. Mirkin, W. Nogala, J. Velmurugan, Y. Wang, Phys. Chem. Chem. Phys. 13 (2011) 21196–21212.
[36] A.J. Wain, Electrochem. Commun. 46 (2014) 9–12.
[37] J.L. Fernandez, D.A. Walsh, A.J. Bard, J. Am. Chem. Soc. 127 (2005) 357–365.
[38] C.M. Sánchez-Sánchez, J. Solla-Gullon, F.J. Vidal-Iglesias, A. Aldaz, V. Montiel, E. Herrero, J. Am. Chem. Soc. 132 (2010) 5622–5624.
[39] C.M. Sánchez-Sánchez, F.J. Vidal-Iglesias, J. Solla-Gullon, V. Montiel, A. Aldaz, J.M. Feliu, E. Herrero, Electrochim. Acta 55 (2010) 8252–8257.
[40] C.M. Sánchez-Sánchez, A.J. Bard, Anal. Chem. 81 (2009) 8094–8100.
[41] L. Johnson, D.A. Walsh, J. Electroanal. Chem. 682 (2012) 45–52.
[42] A.J. Wain, Electrochim. Acta 92 (2013) 383–391.
[43] C.-L. Lin, C.M. Sánchez-Sánchez, A.J. Bard, Electrochem. Solid-State Lett. 11 (2008) B136–B139.
[44] A.R. Zeradjanin, T. Schilling, S. Seisel, M. Bron, W. Schuhmann, Anal. Chem. 83 (2011) 7645–7650.
[45] A. Minguzzi, M.A. Alpuche-Aviles, J. Rodriguez-Lopez, S. Rondinini, A.J. Bard, Anal. Chem. 80 (2008) 4055–4064.
[46] L.-A. Näslund, C.M. Sánchez-Sánchez, A.S. Ingason, J. Backstrom, E. Herrero, J. Rosen, S. Holmin, J. Phys. Chem. C 117 (2013) 6126–6135.
[47] C. Jung, C.M. Sánchez-Sánchez, C.-L. Lin, J. Rodriguez-Lopez, A.J. Bard, Anal. Chem. 81 (2009) 7003–7008.
[48] C.-L. Lin, J. Rodriguez-Lopez, A.J. Bard, Anal. Chem. 81 (2009) 8868–8877.
[49] M. Gomez-Mingot, S. Griveau, F. Bedioui, C.E. Banks, V. Montiel, J. Iniesta, Electrochim. Acta 140 (2014) 42–48.
[50] A. Gennaro, A.A. Isse, C.L. Bianchi, P.R. Mussini, M. Rossi, Electrochem. Commun. 11 (2009) 1932–1935.
[51] M.-C. Daniel, D. Astruc, Chem. Rev. 104 (2004) 293–346.
[52] J. Pérez-Juste, L.M. Liz-Marzán, S. Carnie, D.Y.C. Chan, P. Mulvaney, Adv. Funct. Mater. 14 (2004) 571–579.
[53] G. Frens, Nat. Phys. Sci. 241 (1973) 20–22.
[54] A. Vashkyalis, O. Demontaite, Elektrokhimiya 14 (1978) 1050–1052.
[55] J.W.F. Robertson, D.J. Tiani, J.E. Pemberton, Langmuir 23 (2007) 4651–4661.
[56] D.R. Lide (Ed.), CRC Handbook of Chemistry and Physics, 74th ed., CRC Press, Boca Raton, 1993–1994.

[57] Y. Shao, M.V. Mirkin, J. Phys. Chem. B 102 (1998) 9915–9921.
[58] D.A. Walsh, J.L. Fernandez, J. Mauzeroll, A.J. Bard, Anal. Chem. 77 (2005) 5182–5188.
[59] M. Grzelczak, J. Pérez-Juste, P. Mulvaney, L.M. Liz-Marzán, Chem. Soc. Rev. 37 (2008) 1783–1791.
[60] N.G. Bastús, F. Merkoçi, J. Piella, V. Puntes, Chem. Mater. 26 (2014) 2836–2846.
[61] O.V. Klymenko, O. Buriez, E. Labbè, D.-P. Zhan, S. Rondinini, Z.-Q. Tian, I. Svir, C. Amatore, ChemElectroChem 1 (2014) 227–240.
[62] S. Ardizzone, G. Cappelletti, P.R. Mussini, S. Rondinini, L.M. Doubova, Russ. J. Electrochem. 39 (2003) 170–176.
[63] P.R. Mussini, S. Ardizzone, G. Cappelletti, M. Longhi, S. Rondinini, L.M. Doubova, J. Electroanal. Chem. 552 (2003) 213–221.